Peer reviewed version

Link to publication record in Explore Bristol Research
PDF-document

University of Bristol - Explore Bristol Research
General rights

Sensitivity Images for Multi-View Ultrasonic Array Inspection

Nicolas Budyn[1, a)], Rhodri Bevan[1], Anthony J. Croxford[1], Jie Zhang[1], Paul D. Wilcox[1], Artem Kashubin[2] and Peter Cawley[2]

[1]*Department of Mechanical Engineering, University of Bristol, Bristol, United Kingdom*
[2]*Department of Mechanical Engineering, Imperial College London, United Kingdom*

[a)]Corresponding author: n.budyn@bristol.ac.uk

Abstract. The multi-view total focusing method (TFM) is an imaging technique for ultrasonic full matrix array data that typically exploits ray paths with zero, one or two internal reflections in the inspected object and for all combinations of longitudinal and transverse modes. The fusion of this vast quantity of views is expected to increase the reliability of ultrasonic inspection; however, it is not trivial to determine which views and which areas are the most suited for the detection of a given type and orientation of defect. This work introduces sensitivity images that give the expected response of a defect in any part of the inspected object and for any view. These images are based on a ray-based analytical forward model. They can be used to determine which views and which areas lead to the highest probability of detection of the defect. They can also be used for quantitatively analyzing the effects of the parameters of the inspection (probe angle and position, for example) on the overall probability of detection. Finally, they can be used to rescale TFM images so that the different views have comparable amplitudes. This methodology is applied to experimental data and discussed.

INTRODUCTION

The Total Focusing Method (TFM) is an array imaging algorithm that synthetically focuses the wave front at every point of the image[1]. Multi-view TFM is an extension of TFM that exploits internal reflections and mode conversions[2]. For example, an image can be made with the combination of the longitudinal mode between the transmitter and the image point, the transverse mode between the image point and the backwall and finally the longitudinal mode between the backwall and the receiver. Such a combination of modes between the probe and the inspected area is named a view. The number of possible views is unbounded because the number of internal reflections can be arbitrarily high. Each view creates an image of the inspected object that may contain useful information for detection and characterization. However, manually reviewing a substantial number of images requires more time than conventional inspections, which is a practical issue. Moreover, the views have different sensitivity: each view corresponds to a different way to insonify the inspected object (different amplitudes and angles relative to the defect of the incident and scattered waves); therefore, the ultrasonic response of a defect depends on the view and the defect nature and location. This variation of sensitivity makes the quantitative interpretation of multi-view TFM images difficult without an appropriate model because a scatterer has different amplitudes across different images. To overcome these two challenges, the long-term objective of the authors is to automatically fuse the multi-view TFM images to create a subset of information both easier and faster to review by a human operator or automatically. A requirement is to determine which views and areas give a high-enough scatterer response. To do so, this paper introduces a method to calculate the sensitivity images of multi-view TFM using a ray-based forward model.
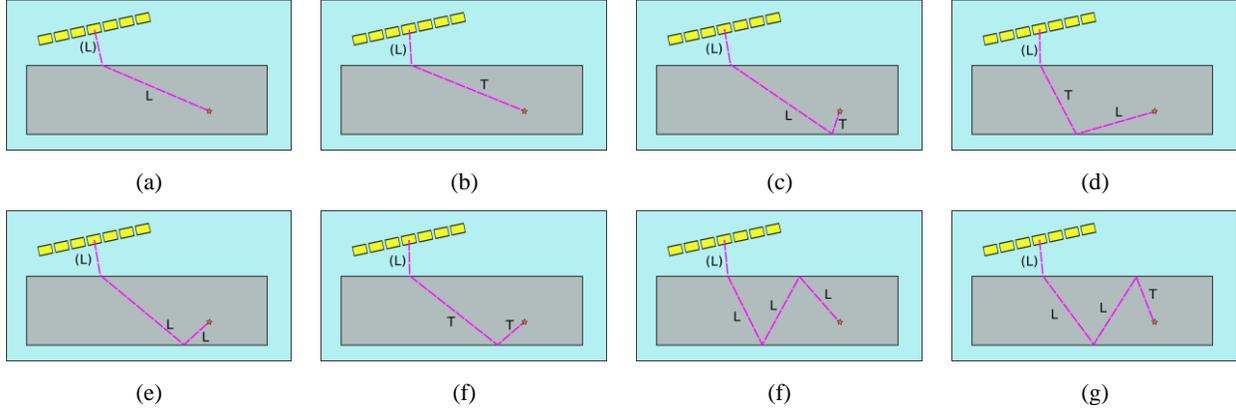
MULTI-VIEW TFM

FIGURE 1. 8 possible ray paths in an immersion set-up between the probe and a scatterer. L stands for longitudinal mode, T for transverse mode. The longitudinal mode propagating in the water is not included in the nomenclature. Transmission nomenclature: direct paths L (a) and T (b), skip paths LT (c), TL (d), LL (e) and TT (f) double skip paths (not exhaustive) LLL (f) and LLT (g). The reception nomenclature is similar but the modes are listed from the scatterer instead of from the probe, for example TLL (g).

   The Full Matrix Capture (FMC) data contains the ultrasonic time-traces of the inspected object for all possible pairs of transmitters and receivers. The scanline obtained for the transmitter i and the receiver j ($i, j = 1 \ldots N$ where N is the number of elements) is denoted $k_{ij}(t)$ in time domain.

   A view is made up of two ray paths: from the probe to the scatterer (transmission) and from the scatterer to the probe (reception). Figure 1 presents paths with zero (direct), one (skip) or two (double skip) internal reflections. In an immersion inspection, the first and the final legs of the total ray path are in water, which only supports longitudinal modes; for the sake of concision, these two L modes are not included in the nomenclature. The view is named after the two paths' names; for example, the view L-TL is made up of the direct path L (transmission nomenclature) from the transmitter to the scatterer, then the path TL (reception nomenclature) from the scatterer to the receiver. The TFM image for a view is defined as:

$$I(r) := \left| \sum_{i,j=1\ldots N} \tilde{k}_{ij}\left(\tau_{ij}(r) \right) \right|$$

   where $\tau_{ij}(r)$ is the time of flight between the transmitter i, the grid point r and the receiver j for the given view (i.e.,ray paths) and where $\tilde{k}_{ij}(t)$ is the analytic signal of $k_{ij}(t)$, obtained with a Hilbert transform.

   Choosing two paths amongst a set of n ray paths gives a total of n^2 views. However, some views produce the same TFM image because the FMC matrix is symmetrical. To demonstrate this property, the time of flight $\tau_{ij}(r) = \tau_i(r) + \tau'_j(r)$ is decomposed as the sum of the time of flight for the transmission path, $\tau_i(r)$, and the reception path, $\tau'_j(r)$. It follows:

$$I(r) = \left| \sum_{i,j=1\ldots N} \tilde{k}_{ij}\left(\tau_i(r) + \tau'_j(r) \right) \right| = \left| \sum_{i,j=1\ldots N} \tilde{k}_{ji}\left(\tau_i(r) + \tau'_j(r) \right) \right| = \left| \sum_{i,j=1\ldots N} \tilde{k}_{ij}\left(\tau_j(r) + \tau'_i(r) \right) \right|$$

   This last expression is the TFM image of the view where the transmission and the reception paths are swapped, for example, L-TL and TL-L. So, the TFM images of these views are rigorously the same. For this reason, amongst the $6^2 = 36$ views that are formed with the 6 direct and skip paths ((a) to (e) in Fig. 1.), only 21 give independent TFM images.

FORWARD MODEL

A 2D ray-based LTI model was implemented for immersion inspection[3]. For a given view, the contribution a scatterer centered in $\mathbf{y}$, insonified by the i-th probe element and received by the j-th element is denoted

$$F_{ij}(\omega, y) = P_{ij}(\omega, y) \exp\left(+\iota\omega\tau_{ij}(y)\right) U(\omega)$$

where $U(\omega)$ is the input pulse, $\tau_{ij}(\mathbf{y})$ the total time of flight between the transmitter, the scatterer and the receiver, and where $P_{ij}(\omega, y)$ contains the transmission and reflection coefficients at the fluid-solid interface(s), the scattering function, the directivity of the probe elements and the geometrical attenuation (beam-spreading). To avoid confusion with the array indices i and j, the imaginary unit is denoted ι (iota). In this paper, the considered scatterer is a side-drilled hole; its scattering function is calculated analytically[4]. The material attenuation and the multiple-scattering are assumed to be negligible. For modelling the wall response, a similar model without the scattering function is used. The FMC data would be modelled as the sum of these scatterer contributions with possibly a multiple-scattering interaction, the wall contributions and additional material noise; this is however not required in this work.

The energy spectral density of the pulse generated by the ultrasonic probe is typically bell-shaped and centered at the probe frequency. Because most of the energy is located close to this frequency, a single frequency approximation of the model is considered:

$$F_{ij}^{\text{sf}}(\omega, y) = P_{ij}(\omega_0\text{sgn}(\omega), y) \exp\left(+\iota\omega\tau_{ij}(y)\right) U(\omega)$$

where ω_0 is the probe center frequency.

SENSITIVITY IMAGE

Definition

The sensitivity image of a view is defined at any point as the TFM intensity that a defect centered at this point yields[5]:

$$E(r) := \left| \sum_{i,j=1\ldots N} \tilde{f}_{ij}\left(\tau_{ij}(r), r\right) \right|$$

where $\tilde{f}_{ij}(t, r)$ is the analytic signal of $f_{ij}(t, r)$, the scatterer contribution defined above. This equation is like the TFM definition except that the time-trace $k_{ij}(t)$ is replaced by the defect contribution $f_{ij}(t, r)$. This definition of the sensitivity ignores the scatterer response from other views than the one considered and the contributions of other scatterers, which are sources of artefacts in multi-view TFM. It also ignores the wall responses. TFM constructively sums the response of a scatterer at its position and destructively any other response. It is assumed the latter summation is negligible with respect to the former at the position of a scatterer. In other words, at the position of a scatterer, the sensitivity as defined above is assumed to be almost equal to the TFM intensity.

The sensitivity equation is rewritten in the frequency domain to bring the forward model out:

$$E(r) = \left| \sum_{i,j=1\ldots N} \frac{1}{2\pi} \int_{-\infty}^{+\infty} \tilde{F}_{ij}(\omega, r) \exp\left(-\iota\omega\tau_{ij}(r)\right) d\omega \right|$$

$$= \left| \sum_{i,j=1\ldots N} \frac{1}{\pi} \int_0^{+\infty} F_{ij}(\omega, r) \exp\left(-\iota\omega\tau_{ij}(r)\right) d\omega \right|$$

$$= \left| \sum_{i,j=1\ldots N} \frac{1}{\pi} \int_0^{+\infty} P_{ij}(\omega, r) U(\omega) d\omega \right|$$

The single-frequency approximation gives:

$$E^{\text{sf}}(r) = \left| \sum_{i,j=1\ldots N} \frac{1}{\pi} \int_0^{+\infty} P_{ij}(\omega_0, r) U(\omega) d\omega \right|$$

Finally, using the definition of an analytic signal and the direct Fourier transform, it follows:

$$E^{\text{sf}}(r) = \left| \tilde{u}(0) \sum_{i,j=1\ldots N} P_{ij}(\omega_0, r) \right|$$

The term $|\tilde{u}(0)|$ is the envelope of the input signal $u(t)$ at the time $t = 0$. In a well set-up experiment (no instrumentation delay), it is the maximum value of the envelope. In practice, it acts as a scaling coefficient between the experimental intensities and the unscaled sensitivity images. In this paper, this coefficient is determined using the first front wall echo in the experimental pulse-echo time-traces. This signal is used because it has an excellent signal-to-noise ratio. Their theoretical amplitudes are calculated with the forward model up to a multiplicative factor, which is exactly $|\tilde{u}(0)|$. The scaling coefficient is obtained by taking the ratio of the experimental intensity by the theoretical one. Thus, one estimation per pulse-echo scanline is made; the final value is obtained by performing an ordinary least-square regression for robustness.
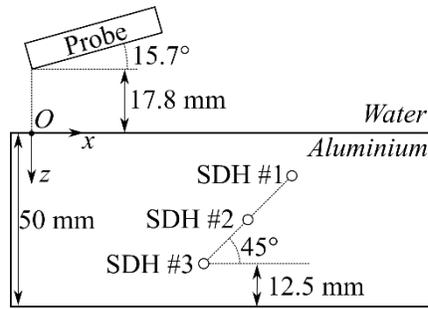
Example of Sensitivity Images

FIGURE 2. Drawing of the immersion inspection set-up, used for the calculation of sensitivity images and the experimental validation. The locations of the SDH is irrelevant to the sensitivity images, where by definition each pixel is a defect center.
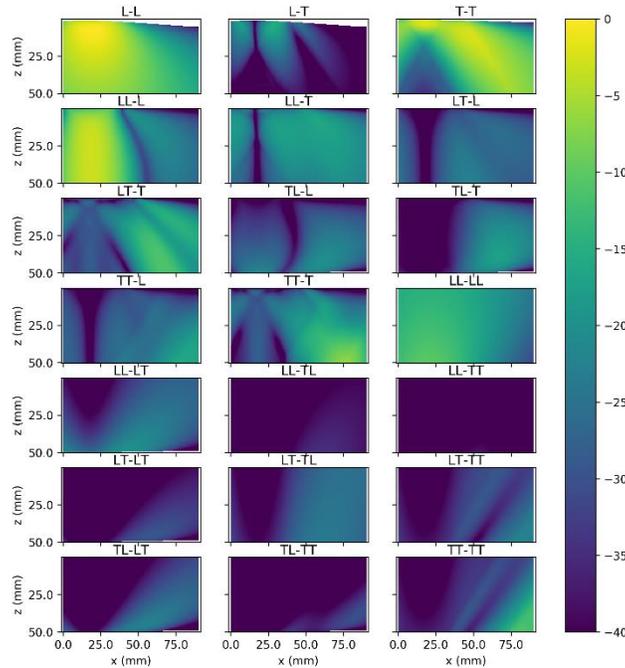

FIGURE 3. Sensitivity images (dB) for a side-drilled hole of diameter 1 mm.

An example of sensitivity images for the inspection of side-drilled holes (SDH) is shown in Fig. 3. Figure 2 describes the set-up. The probe is a 128-element 5-MHz linear array (element pitch of 0.3 mm). The inspected object is a 50-mm thick aluminium block. The considered defect is a side-drilled hole of diameter 1 mm. Each point of the sensitivity image gives the TFM intensity of a SDH centered on this location. The sensitivity varies greatly (more than 40 dB) within the views and across the views. Most have a blind spot below the probe (strips or areas of below -40 dB). 18,281 possible locations are considered per view. The sensitivity images were computed in around 5 minutes with a workstation with an Intel i7 4790 CPU. These sensitivity images can be used to quantitatively determine which views and areas give a high-enough scatterer response for a given inspection. For example, for detecting an SDH around $x = 60$ mm and $z = 25$ mm (location of SDH #2), the views T-T, L-L and LT-T may be the most appropriate because they give the highest scatterer response. Conversely, the sensitivity images can be a valuable tool to determine the probe and the probe location that give the best results for inspecting a given area with multi-view TFM.
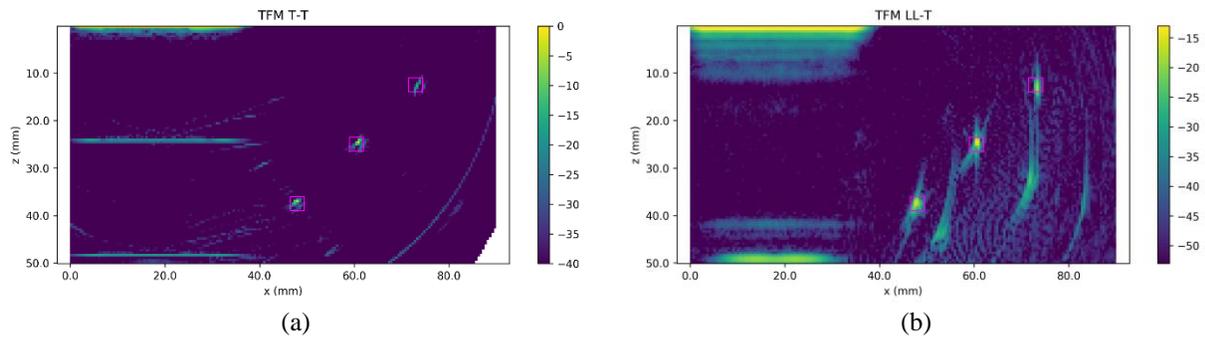
EXPERIMENTAL VALIDATION

(a) (b)

FIGURE 4. Experimental TFM images in dB of the views T-T (a) and LL-T (b). The magenta squares (side 3 mm) show the locations of the SDHs and defines the area of measurements of their intensities. The same dB scale is used for the two figures; the upper limit of the scale is the maximum intensity in the squares; the lower limit is the upper limit minus 40 dB.

To validate the sensitivity images, an experimental acquisition in the set-up described above was performed. The inspected object is an aluminium block ($50 \times 25 \times 208$ mm) with three side-drilled holes (Fig. 2). The probe, whose characteristics are described in the previous section, was manufactured by Imasonic (Besançon, France). The inspected object and the probe are fully immersed in a water tank. The theoretical intensities are compared against the ones measured on experimental TFM images (Fig. 4). The measurements are the maximum intensities in a square of 3 mm side around the defect.
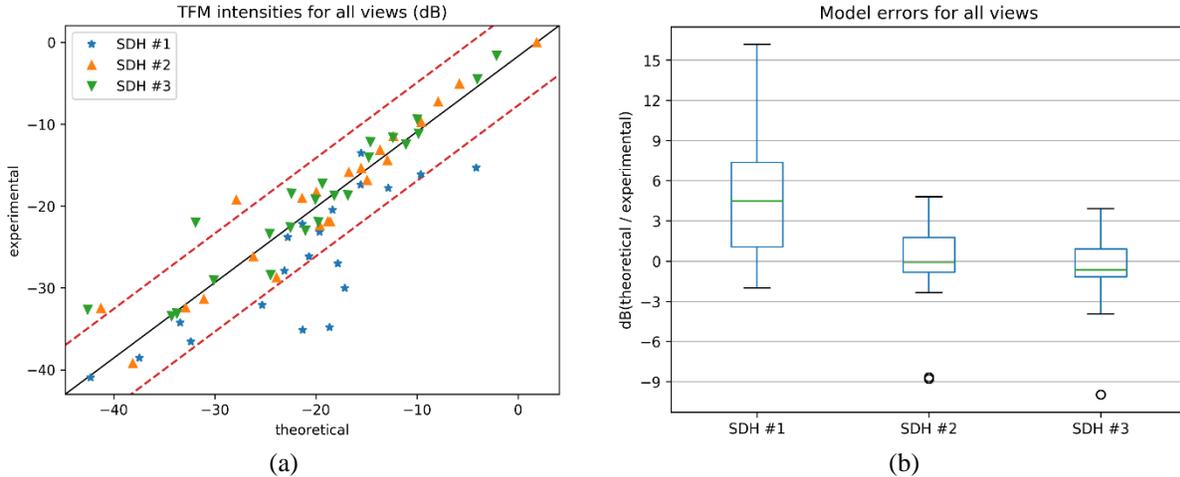
FIGURE 5. Experimental comparison for the three side-drilled holes and 23 views: 21 views obtained from the six direct and skip paths, plus LLL-L and LLL-T. (a): amplitudes on an XY plot. (b): box plot of the errors in dB. The limits of the boxes are the quartile Q1 and Q3, its center is the median, the whiskers are at 1.5 times the interquartile range.

The results are presented in Fig. 5. There are three missing points where imaging could not be performed because the time-traces were too short in time. Most of the theoretical intensities are within ± 6 dB of the experimental ones. The agreement is significantly better for SDH #2 and #3 than for SDH #1. The intensities for SDH #1 are overestimated by the model (median error of +4.5 dB). Given that the ray paths between the probe and this SDH are the longest, this suggests the attenuation due to the propagation length is underestimated in the model: the hypotheses of a negligible material attenuation and/or a 2D beam-spreading may be invalid.

Possible explanations for the errors include the single-frequency approximation, the 2D approximation, the variability of the sensitivity of the piezoelectric elements, the lack of material attenuation, the presence of imaging artefacts (walls and other defects).

CONCLUSION

Sensitivity images for the immersion inspection of side-drilled holes with multi-view TFM were calculated using a 2D ray-based analytical model. A single-frequency approximation is made to reduce the computation time. An experimental validation was performed using a block with three SDHs. There is a ± 6 dB agreement for most views. The errors are significantly larger on SDH, which suggests a systematic underestimation of the wave propagation attenuation. The computation time of these sensitivity images is around 5 minutes. The sensitivity images show which views and areas give the highest scatterer response in multi-view TFM. They can therefore be used for selecting the most sensible views and areas, possibly automatically. In that regard, they are a step toward the fusion of multi-view TFM images for more automated and reliable inspections, which is the long-term objective of the authors.

ACKNOWLEDGMENTS

REFERENCES

[1] C. Holmes, B.W. Drinkwater, and P.D. Wilcox, *NDT E Int*. **38**, 701 (2005).

[2] J. Zhang, B.W. Drinkwater, P.D. Wilcox, and A.J. Hunter, *NDT E Int*. **43**, 123 (2010).

[3] L.W. Schmerr, *Fundamentals of Ultrasonic Nondestructive Evaluation: A Modeling Approach*, 2nd ed., Springer, New York, New York, (2016).

[4] A.L. Lopez-Sanchez, H.-J. Kim, L.W. Schmerr, and A. Sedov, J. Nondestruct. Eval. **24**, 83 (2005).

[5] T. Stratoudaki, M. Clark, and P.D. Wilcox, *Opt. Express* ,**24**, 21921 (2016).